Journal of Applied Physics ARTICLE scitation.org/journal/jap

Impact of dislocations on the thermal conductivity of gallium nitride studied by time-domain thermoreflectance

Cite as: J. Appl. Phys. **126**, 185103 (2019); doi: 10.1063/1.5126970
Submitted: 9 September 2019 · Accepted: 27 October 2019 ·
Published Online: 11 November 2019

View Online Export Citation CrossMark

Kihoon Park[1,2] and Can Bayram[1,2,a)]

AFFILIATIONS

[1]Department of Electrical and Computer Engineering, University of Illinois at Urbana-Champaign, Urbana, Illinois 61801, USA
[2]Nick Holonyak, Jr. Micro and Nanotechnology Laboratory, University of Illinois at Urbana-Champaign, Urbana, Illinois 61801, USA

[a)]Innovative COmpound semiconductoR LABoratory (ICORLAB). **Email:** cbayram@illinois.edu. **URL:** https://icorlab.ece.illinois.edu. **Telephone:** +1 (217) 300-0978. **Fax:** +1 (217) 244-6375.

ABSTRACT

GaN thermal conductivity (κ_{GaN}) of hydride vapor phase epitaxy grown GaN (HVPE GaN), high nitride pressure grown GaN (HNP GaN), and metal-organic chemical vapor deposition grown GaN on sapphire (GaN/sapphire) and on Si(111) (GaN/Si) are measured as 204.7 (±4.6), 206.6 (±6.8), 191.5 (±10.5), and 164.4 (±3.2) W/m K, respectively, using the time-domain thermoreflectance technique. Dislocation densities (σ_D) of HVPE GaN, HNP GaN, GaN/sapphire, and GaN/Si are measured as 4.80 $(\pm 0.42) \times 10^5$, 3.81 $(\pm 0.08) \times 10^6$, 2.43 $(\pm 0.20) \times 10^8$, and 1.10 $(\pm 0.10) \times 10^9$ cm^{-2}, respectively, using cathodoluminescence and X-ray diffraction studies. Impurity concentrations of Si, H, C, and O are measured by secondary ion mass spectroscopy studies. The relationship between κ_{GaN} and σ_D is modeled through a new empirical model $\kappa_{GaN} = 210 \tanh^{0.12}(1.5 \times 10^8/\sigma_D)$. A modified Klemens's model, where dislocation induced scattering strength is increased, is proposed to explain the experimental rate of decrease in κ_{GaN} with increasing σ_D. Overall, this work reports how κ_{GaN} of heteroepitaxially-grown GaN can be estimated based on σ_D, providing key design guidelines for thermal management in GaN semiconductor devices.

I. INTRODUCTION

Gallium nitride (GaN) semiconductors are of great interest in photonics and electronics. In solid-state lighting, (In)GaN-based light emitting diodes (LEDs) revolutionized general lighting and are driven with power densities exceeding 100 W/cm^2.[1] In emerging wireless networks, (Al)GaN/GaN high electron mobility transistors (HEMTs) are leading in 5G efforts, and their power densities are projected to reach 60 W/mm.[2] GaN-based devices can sustain such high-power densities thanks to GaN's high thermal stability (<500 °C)[3] and high thermal conductivity (theoretical upper bound being >336 W/m K).[4,5] Yet, GaN thermal conductivity κ_{GaN} is reported to range from 110 to 269 W/m K, suggesting strong dependence on not only growth methods and conditions but also measurement techniques and assumptions.[6–12] For instance, freestanding GaN substrates grown by hydride vapor phase epitaxy (HVPE) and the ammonothermal method reportedly have higher thermal conductivities.[9,10,12] However, most GaN layers are grown on non-native substrates for reduced cost, high scalability, and integrated functionality, and a complete study of such heterogeneously-grown GaN is lacking.[13] It is thus important to explore thermal conductivities of such GaN-on-foreign substrates so that LED and HEMT researchers can create accurate thermoelectrical modeling for thermal management studies.[14,15]

II. GaN THERMAL CONDUCTIVITY

Here, we report a time-domain thermoreflectance (TDTR) study of thermal conductivities of four types of *c*-plane GaN: (1) 350-μm-thick freestanding GaN grown by hydride vapor phase epitaxy (HVPE), (2) 350-μm-thick freestanding GaN grown by high nitride pressure (HNP), (3) 4.5-μm-thick GaN grown on the sapphire substrate by metal-organic chemical vapor phase deposition (MOCVD), and (4) 5-μm-thick GaN grown on

the Si(111) substrate by MOCVD with step-graded $Al_xGa_{1-x}N$ and AlN buffer layers in between [i.e., 5-μm-thick GaN/400-nm-thick $Al_{0.33}Ga_{0.67}N$/290-nm-thick $Al_{0.60}Ga_{0.40}N$/200-nm-thick $Al_{0.82}Ga_{0.18}N$/240-nm-thick AlN/Si(111)].[16]

TDTR setup uses a mode-locked Ti:sapphire laser that generates 783 nm laser pulses at an 80 MHz repetition rate as the light source. The laser pulses are split into pump and probe beams. The pump laser beam is modulated by an electro-optical modulator and passes through a mechanical delay stage where its arrival time at the sample is controlled. The laser modulation frequency is set to 11 MHz, and the mechanical delay stage introduces up to 3.6 ns of delay with respect to the probe laser beam. The probe laser beam is modulated by a chopper that operates at 200 Hz to suppress coherent laser signal pickup. A fast-response photodiode detector coupled with a radio-frequency (RF) lock-in amplifier is then used to pick up the reflected laser signal. The RF lock-in amplifier has outputs of an in-phase V_{in} signal and an out-of-phase V_{out} signal at the laser modulation frequency. The ratio $-V_{in}/V_{out}$ is fit to the one-dimensional thermal transport model from an analytical solution for heat flow in a multilayered structure.[17] Fitting is done by minimizing the sum of the squares of error between the thermal transport model and measurement data while sweeping through a range of κ_{GaN} and Al/GaN thermal boundary resistance (TBR).[18] Throughout the analyses in this work, the sensitivities of the fitting parameters are closely monitored to ensure the fittings are valid.[19] A laser spot size ($1/e^2$ radius) of 10.6 μm and a modulation frequency of 11 MHz create a thermal penetration depth (~1.4 μm)—much smaller than the GaN layer thicknesses (~4.5 μm) and the ratio of the lateral heat spread and thermal penetration depth is large enough (>4), allowing the use of the one-dimensional thermal transport model,[20,21] and ignoring any thermal conductivity anisotropy.[22,23]

A thin layer of aluminum (Al) is deposited by dc magnetron sputtering on each sample to serve as a transducer.[24] Al film thicknesses (h_{Al}) (~100 nm) are obtained from the picosecond acoustics echo observed at the short time delay (<100 ps) part of the TDTR measurement while assuming a longitudinal speed of sound $v_l = 6.42$ nm/ps and a 3-nm-thick native oxide layer accordingly: $h_{Al} = 6.42 \times t_{echo}/2 + 3$, where t_{echo} is the arrival time of the first echo. Al film thicknesses are also verified using X-ray reflectivity (XRR) measurements and simulations. Thermal conductivities of the deposited Al films are obtained using a four-point probe measurement. Volumetric heat capacity of Al[25] and GaN[11,26] is taken from the literature as $C_{P,Al} = 2.43$ J/cm^{3}K and $C_{P,GaN} = 2.64$ J/cm^{3}K, respectively.

Figure 1 shows actual TDTR measurement data (open symbols) and thermal transport model calculations along with key experimental parameters for (a) HVPE GaN, (b) HNP GaN, (c) GaN/sapphire, and (d) GaN/Si samples. A good fit is achieved with the coefficient of determination (i.e., R^2) >0.97, and Al/GaN interfaces have consistent TBRs (~10 m^{2}K/GW) across samples. The thermal transport model calculation with $\kappa_{GaN} \pm 10\%$ is also plotted (dashed lines). Most of the actual TDTR measurement data points are within the $\kappa_{GaN} \pm 10\%$ curves throughout the entire time delay, indicating that the uncertainties of the measurements are relatively small and that the sensitivities of the κ_{GaN} data are sufficiently large, ensuring a valid fitting. Multiple TDTR

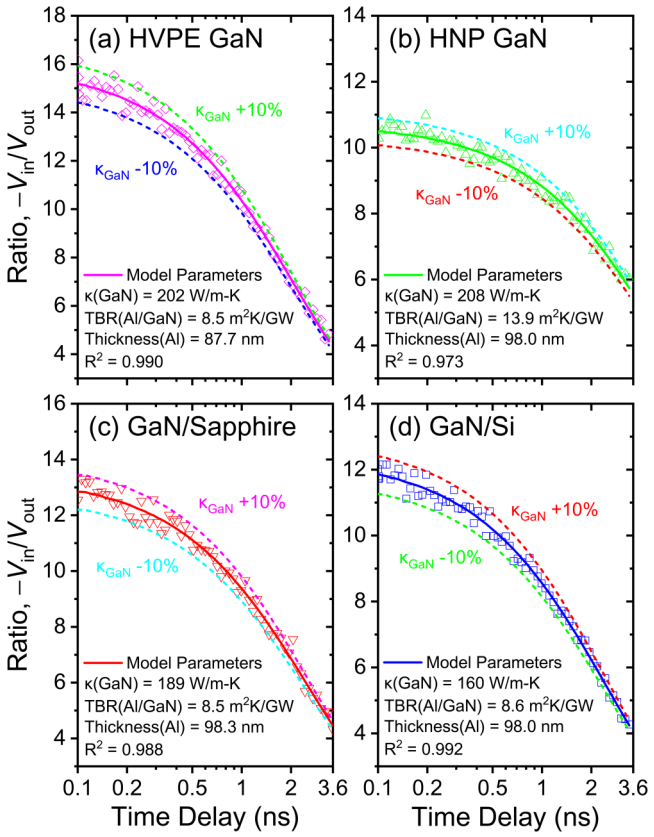

FIG. 1. TDTR measurement results ($-V_{in}/V_{out}$ as a function of time delay) and fitted κ_{GaN} of (a) HVPE GaN, (b) HNP GaN, (c) GaN/sapphire, and (d) GaN/Si are plotted. Open symbols indicate measurement data, solid lines indicate thermal transport model calculation (with fitting parameters listed), and dashed lines indicate thermal transport model calculation with $\kappa_{GaN} \pm 10\%$.

measurements are done on each sample to obtain average κ_{GaN}. The results are tabulated in Table I. HVPE and HNP GaN exhibit a relatively high κ_{GaN} of 204.7 (±4.6) and 206.6 (±6.8) W/m K, respectively, GaN/sapphire exhibits a moderate κ_{GaN} of 191.5 (±10.5) W/m K, and GaN/Si exhibits the lowest κ_{GaN} of 164.4 (±3.2) W/m K. κ_{GaN} of HVPE and HNP GaN are statistically indistinguishable; yet compared to that of the GaN/Si sample, they are larger by ~25%.

III. GaN MATERIAL CHARACTERIZATION

To explore the origins of κ_{GaN} differences among the samples, dislocation densities (σ_D) are measured using cathodoluminescence (CL). Figure 2 shows CL images of (a) HVPE GaN, (b) HNP GaN, (c) GaN/sapphire, and (d) GaN/Si samples, taken in a panchromatic view with an acceleration voltage of 5 kV. As non-radiative recombination centers, dislocations appear as dark spots, which are then counted for density calculations.[27] Five measurements per sample are collected. HVPE GaN, HNP

TABLE I. Dislocation densities σ_D (measured by CL and XRD), impurity concentrations (measured by SIMS), impurity scattering strengths Γ (calculated by Klemens's model), and GaN thermal conductivities κ_{GaN} (measured by TDTR) of HVPE GaN, HNP GaN, GaN/sapphire, and GaN/Si are tabulated.

	σ_D ($\times 10^8$ cm^{-2})		Impurity concentration (cm^{-3})					
Sample	CL	XRD	Si	H	C	O	Γ	κ_{GaN} (W/m K)
HVPE GaN	0.005	0.018	9.0×10^{16}	8.3×10^{15}	7.7×10^{16}	7.6×10^{15}	6.82×10^{-7}	204.7 ± 4.6
HNP GaN	0.038	0.593	3.0×10^{17}	8.1×10^{15}	8.0×10^{16}	7.4×10^{15}	9.56×10^{-7}	206.6 ± 6.8
GaN/sapphire	2.433	2.562	4.5×10^{15}	2.4×10^{17}	1.3×10^{17}	1.6×10^{16}	3.44×10^{-6}	191.5 ± 10.5
GaN/Si	10.993	14.671	1.6×10^{15}	1.6×10^{17}	8.7×10^{18}	1.1×10^{16}	5.81×10^{-5}	164.4 ± 3.2

GaN, GaN/sapphire, and GaN/Si samples have an average σ_D of 4.80 $(\pm 0.42) \times 10^5$, 3.81 $(\pm 0.08) \times 10^6$, 2.43 $(\pm 0.20) \times 10^8$, and 1.10 $(\pm 0.10) \times 10^9$ cm^{-2}, respectively (Table I). Additionally, X-ray diffraction (XRD) (0002) symmetric and (10$\bar{1}$2) asymmetric ω scans are performed to verify σ_D. Based on the full-width-at-half-maximum (FWHM) of the (0002) and (10$\bar{1}$2) ω scans, screw-type and edge-type σ_D are calculated[16,28] (see the supplementary material) and tabulated in Table I. For the GaN/sapphire and GaN/Si samples, both techniques reveal similar σ_D. For the HVPE and HNP GaN samples, XRD estimates a higher σ_D than the CL technique. We believe that the discrepancy in this case is most likely due to the limitations of the FWHM-based XRD σ_D calculation model in which it is assumed that the crystal forms a mosaic structure consisting of similar-sized blocks.[29] For samples with low σ_D, the dislocations form in clusters making it difficult to assume that there exists a constant lateral coherence length between dislocations.[27,30]

A secondary ion mass spectroscopy (SIMS) is performed to estimate the impurity concentrations in the GaN samples. The concentrations of Si, H, C, and O are measured and are then used to quantify the "scattering strength" Γ through Klemens's model $\Gamma = \sum_i f_i[1 - M_i/\bar{M}]^2$, where f_i is the fractional concentration of the ith impurity atom, M_i is the atomic mass of the ith impurity atom, and $\bar{M}$ is the average atomic mass. Both measured impurity concentrations and calculated Γ values are tabulated in Table I. The largest Γ obtained from the GaN/Si sample is still a factor of five times smaller than the scattering due to naturally occurring isotopes ($\Gamma_{isotope} = 2.744 \times 10^{-4}$), suggesting that impurity concentrations of these samples in this work will not limit κ_{GaN} (see the

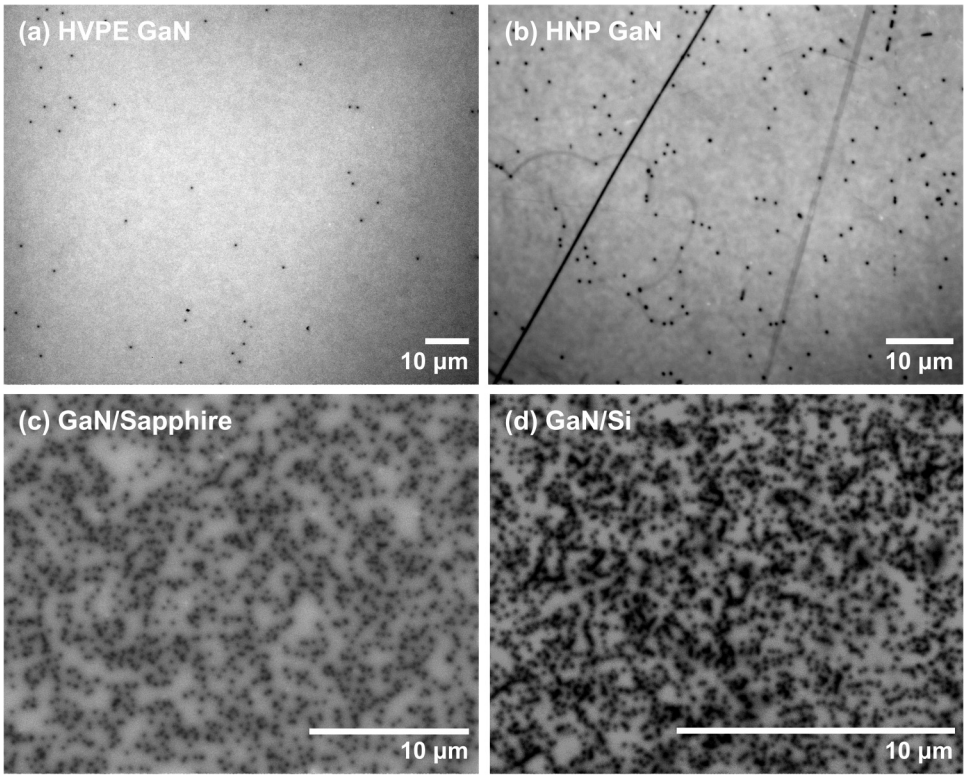

FIG. 2. CL images of (a) HVPE GaN, (b) HNP GaN, (c) GaN/sapphire, and (d) GaN/Si are shown. Dislocations are revealed as dark spots and counted by averaging five measurements per sample as 4.80 $(\pm 0.42) \times 10^5$, 3.81 $(\pm 0.08) \times 10^6$, 2.43 $(\pm 0.20) \times 10^8$, and 1.10 $(\pm 0.10) \times 10^9$ cm^{-2}, respectively.

supplementary material for SIMS measurement data and discussion).

IV. RESULTS AND DISCUSSION

Figure 3 plots experimentally measured κ_{GaN} as a function of experimentally measured σ_D (open symbols). An earlier empirical model (plotted as a dotted line for reference) by Mion *et al.*,[31] expressed as $\kappa_{GaN} = 230 \tanh^{0.12}(5 \times 10^6/\sigma_D)$, fails to provide a good fit to this work. A new empirical model, $\kappa_{GaN} = 210 \tanh^{0.12}(1.5 \times 10^8/\sigma_D)$, is proposed in this work (plotted as a dashed line for comparison). The two empirical models have two major differences. The first difference is the maximum κ_{GaN} employed in the empirical formula. In the literature, highest reported κ_{GaN} values are 294 (±44) and 253 (±22) W/m K (measured by the laser flash method)[32,33] and 269 W/m K (measured by the stationary heat flow method).[8] Yet, most of κ_{GaN} are reportedly <230 W/m K.[10,22,31,34–36] In close context to this work, Zheng *et al.*[23] recently studied high quality HVPE and ammonothermal GaN using the TDTR technique and reported a κ_{GaN} of ~209 W/m K. These results suggest that the discrepancy of measured maximum κ_{GaN} may arise from the differences in the employed experimental technique. The second difference is the deflection point where κ_{GaN} starts to drop as a function of σ_D. In our modified empirical model, the σ_D level at which κ_{GaN} starts to drop rapidly is chosen as 1.5×10^8 cm^{-2}—a slightly larger value from that in Mion *et al.*[31] (i.e., 5×10^6 cm^{-2}). With this shift, the new empirical model in this work properly captures not only our experimental data on the GaN/sapphire and GaN/Si samples but also other literature that studied GaN samples with high σ_D (>10^8 cm^{-2}).[37–39]

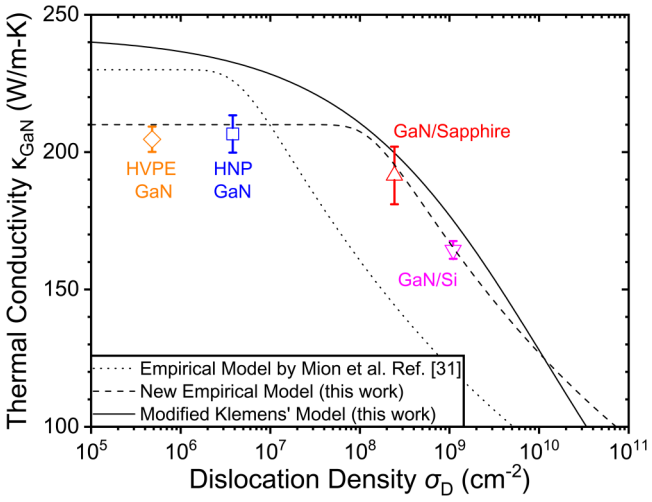

FIG. 3. κ_{GaN} of HVPE GaN, HNP GaN, GaN/sapphire, and GaN/Si as a function of σ_D are plotted (open symbols). The empirical model by Mion *et al.* from Ref. 31 $\kappa_{GaN} = 230 \tanh^{0.12}(5 \times 10^6/\sigma_D)$ (dotted line); new empirical model, $\kappa_{GaN} = 210 \tanh^{0.12}(1.5 \times 10^8/\sigma_D)$ (dashed line, this work); and modified Klemens's model (solid line, this work) are plotted together for comparison.

Based on the experimental data, we propose to modify Klemens's model to explain the findings. The original Klemens's model describes the effect of σ_D on κ_{GaN} by the functions[5,40]

$$\frac{1}{\tau_{DC}} = \eta \sigma_D \frac{V_0^{4/3}}{v^2} \omega^3, \tag{1}$$

$$\frac{1}{\tau_S} = \frac{2^{3/2}}{3^{7/2}} \eta \sigma_D b_S^2 \gamma^2 \omega, \tag{2}$$

$$\frac{1}{\tau_E} = \frac{2^{3/2}}{3^{7/2}} \eta \sigma_D b_E^2 \gamma^2 \omega \left\{ \frac{1}{2} + \frac{1}{24} \left(\frac{1-2\nu}{1-\nu} \right)^2 \left[1 + \sqrt{2} \left(\frac{v_L}{v_T} \right)^2 \right]^2 \right\}, \tag{3}$$

where τ_{DC} is the phonon scattering relaxation time associated with dislocation cores, η is the weight factor to account for the mutual orientation of the direction of the temperature gradient and the dislocation line, V_0 is the volume per atom, v is the polarization-averaged phonon velocity, v_L (v_T) is the longitudinal (transverse) sound velocity, ω is the phonon frequency, τ_S (τ_E) is the phonon relaxation time associated with screw-type (edge-type) dislocations, b_S (b_E) is the screw-type (edge-type) dislocation Burgers vector, and γ is the Gruneisen parameter. Previously published literature[11,31,34] agrees that the impact of σ_D on κ_{GaN} is underestimated. In order to compensate for the discrepancy, a correction factor of 1000 is commonly used as a multiplier to the scattering rates to fit the experimental results.[11,34]

To fit our experimental data, Klemens's model is modified accordingly: η is set as 2×10^{10} and σ_D is replaced by $\sigma_D^{0.4}$. The η should be considered as a correction factor rather than a factor that purely represents the effect of the relative orientation between the temperature gradient and the dislocation. These two modifications effectively increase the strength of phonon–dislocation scattering and adjust the rate of κ_{GaN} decrease such that κ_{GaN} is not vanishingly small (>35 W/m K) at $\sigma_D > 10^{10}$ cm^{-2}.[6,7,31] This modified Klemens's model is plotted in Fig. 3 (solid line). The basic GaN material parameters are taken from Ref. 5. The same parameter set is used for the calculations of all four GaN samples.

V. CONCLUSION

In conclusion, four types of GaN samples (HVPE GaN, HNP GaN, GaN/sapphire, and GaN/Si) are studied using XRD and TDTR to determine σ_D and κ_{GaN}, respectively. κ_{GaN} of HVPE GaN, HNP GaN, GaN/sapphire, and GaN/Si are measured as 204.7 (±4.6), 206.6 (±6.8), 191.5 (±10.5), and 164.4 (±3.2) W/m K, respectively. The determining factor of κ_{GaN} is shown to be σ_D when $\sigma_D > 1.5 \times 10^8$ cm^{-2}. The new empirical model $\kappa_{GaN} = 210 \tanh^{0.12}(1.5 \times 10^8/\sigma_D)$ describes the relationship between κ_{GaN} and σ_D. A modified Klemens's model is proposed to increase the strength of phonon–dislocation scattering and adjust the rate of κ_{GaN} decrease such that it explains the experimental results. Overall, we report how κ_{GaN} of heteroepitaxial GaN can be estimated based on σ_D. Our work lays the foundation in thermal management of the technologically important GaN-based semiconductor devices, typically grown on foreign substrates with high σ_D.

SUPPLEMENTARY MATERIAL

The laser power dependent TDTR measurement results, XRD ω scans in the (0002) symmetric and (10$\bar{1}$2) asymmetric planes for dislocation density determination, and the SIMS measurement results are discussed in detail in the supplementary material.

ACKNOWLEDGMENTS

This work was supported by the Air Force Office of Scientific Research (AFOSR) through Young Investigator Program Grant No. FA9550-16-1-0224 and was carried out in the Nick Holonyak, Jr. Micro and Nanotechnology Laboratory and Frederick Seitz Materials Research Laboratory Central Research Facilities, the University of Illinois at Urbana-Champaign, IL, USA.

REFERENCES

[1]M. Ha and S. Graham, Microelectron. Reliab. **52**, 836 (2012).
[2]Y.-F. Wu, M. Moore, A. Saxler, T. Wisleder, and P. Parikh, in *2006 64th Device Research Conference* (IEEE, 2006), p. 151.
[3]D. Maier, M. Alomari, N. Grandjean, J. F. Carlin, M. A. Diforte-Poisson, C. Dua, A. Chuvilin, D. Troadec, C. Gaquière, U. Kaiser, S. L. Delage, and E. Kohn, IEEE Trans. Device Mater. Reliab. **10**, 427 (2010).
[4]L. Lindsay, D. A. Broido, and T. L. Reinecke, Phys. Rev. Lett. **109**, 095901 (2012).
[5]J. Zou, D. Kotchetkov, A. A. Balandin, D. I. Florescu, and F. H. Pollak, J. Appl. Phys. **92**, 2534 (2002).
[6]D. I. Florescu, V. M. Asnin, F. H. Pollak, R. J. Molnar, and C. E. C. Wood, J. Appl. Phys. **88**, 3295 (2000).
[7]D. I. Florescu, V. M. Asnin, F. H. Pollak, A. M. Jones, J. C. Ramer, M. J. Schurman, and I. Ferguson, Appl. Phys. Lett. **77**, 1464 (2000).
[8]A. Jezowski, O. Churiukova, J. Mucha, T. Suski, I. A. Obukhov, and B. A. Danilchenko, Mater. Res. Express **2**, 085902 (2015).
[9]R. Rounds, B. Sarkar, T. Sochacki, M. Bockowski, M. Imanishi, Y. Mori, R. Kirste, R. Collazo, and Z. Sitar, J. Appl. Phys. **124**, 105106 (2018).
[10]M. Slomski, P. P. Paskov, J. H. Leach, J. F. Muth, and T. Paskova, Phys. Status Solidi B **254**, 1600713 (2017).
[11]T. E. Beechem, A. E. McDonald, E. J. Fuller, A. A. Talin, C. M. Rost, J.-P. Maria, J. T. Gaskins, P. E. Hopkins, and A. A. Allerman, J. Appl. Phys. **120**, 095104 (2016).
[12]A. Jezowski, B. A. Danilchenko, M. Boćkowski, I. Grzegory, S. Krukowski, T. Suski, and T. Paszkiewicz, Solid State Commun. **128**, 69 (2003).
[13]K. T. Lee, C. Bayram, D. Piedra, E. Sprogis, H. Deligianni, B. Krishnan, G. Papasouliotis, A. Paranjpe, E. Aklimi, K. Shepard, T. Palacios, and D. Sadana, IEEE Electron Device Lett. **38**, 1094 (2017).
[14]K. Park and C. Bayram, Appl. Phys. Lett. **109**, 151904 (2016).
[15]A. Sarua, H. Ji, K. P. Hilton, D. J. Wallis, M. J. Uren, T. Martin, and M. Kuball, IEEE Trans. Electron Devices **54**, 3152 (2007).
[16]H.-P. Lee, J. Perozek, L. D. Rosario, and C. Bayram, Sci. Rep. **6**, 37588 (2016).
[17]D. G. Cahill, Rev. Sci. Instrum. **75**, 5119 (2004).
[18]J. Yang, E. Ziade, and A. J. Schmidt, Rev. Sci. Instrum. **87**, 014901 (2016).
[19]P. Jiang, X. Qian, and R. Yang, J. Appl. Phys. **124**, 161103 (2018).
[20]P. Jiang, X. Qian, and R. Yang, Rev. Sci. Instrum. **88**, 074901 (2017).
[21]J. Liu, J. Zhu, M. Tian, X. Gu, A. Schmidt, and R. Yang, Rev. Sci. Instrum. **84**, 034902 (2013).
[22]E. Ziade, J. Yang, G. Brummer, D. Nothern, T. Moustakas, and A. J. Schmidt, Appl. Phys. Lett. **110**, 031903 (2017).
[23]Q. Zheng, C. Li, A. Rai, J. H. Leach, D. A. Broido, and D. G. Cahill, Phys. Rev. Mater. **3**, 014601 (2019).
[24]Y. Wang, J. Y. Park, Y. K. Koh, and D. G. Cahill, J. Appl. Phys. **108**, 043507 (2010).
[25]E. H. Buyco and F. E. Davis, J. Chem. Eng. Data **15**, 518 (1970).
[26]B. A. Danilchenko, T. Paszkiewicz, S. Wolski, A. Jezowski, and T. Plackowski, Appl. Phys. Lett. **89**, 061901 (2006).
[27]S. J. Rosner, E. C. Carr, M. J. Ludowise, G. Girolami, and H. I. Erikson, Appl. Phys. Lett. **70**, 420 (1997).
[28]R. Liu, C. McCormick, and C. Bayram, AIP Adv. **9**, 025306 (2019).
[29]M. A. Moram and M. E. Vickers, Rep. Prog. Phys. **72**, 036502 (2009).
[30]T. Metzger, R. Höpler, E. Born, O. Ambacher, M. Stutzmann, R. Stömmer, M. Schuster, H. Göbel, S. Christiansen, M. Albrecht, and H. P. Strunk, Philos. Mag. A **77**, 1013 (1998).
[31]C. Mion, J. F. Muth, E. A. Preble, and D. Hanser, Appl. Phys. Lett. **89**, 092123 (2006).
[32]E. Richter, M. Gründer, B. Schineller, F. Brunner, U. Zeimer, C. Netzel, M. Weyers, and G. Tränkle, Phys. Status Solidi C **5**, 1450 (2011).
[33]H. Shibata, Y. Waseda, H. Ohta, K. Kiyomi, K. Shimoyama, K. Fujito, H. Nagaoka, Y. Kagamitani, R. Simura, and T. Fukuda, Mater. Trans. **48**, 2782 (2007).
[34]P. P. Paskov, M. Slomski, J. H. Leach, J. F. Muth, and T. Paskova, AIP Adv. **7**, 095302 (2017).
[35]R. B. Simon, J. Anaya, and M. Kuball, Appl. Phys. Lett. **105**, 202105 (2014).
[36]W. Liu, A. A. Balandin, C. Lee, and H. Y. Lee, Phys. Status Solidi A **202**, R135 (2005).
[37]C. Luo, D. R. Clarke, and J. R. Dryden, J. Electron. Mater. **30**, 138 (2001).
[38]J. Cho, Y. Li, W. E. Hoke, D. H. Altman, M. Asheghi, and K. E. Goodson, Phys. Rev. B **89**, 115301 (2014).
[39]C. Y. Luo, H. Marchand, D. R. Clarke, and S. P. Denbaars, Appl. Phys. Lett. **75**, 4151 (1999).
[40]D. Kotchetkov, J. Zou, A. A. Balandin, D. I. Florescu, and F. H. Pollak, Appl. Phys. Lett. **79**, 4316 (2001).

Supplementary Online Material for:

Impact of dislocations on the thermal conductivity of gallium nitride studied by time-domain thermoreflectance

Kihoon Park[1,2] and Can Bayram[1,2a]

[1]*Department of Electrical and Computer Engineering, University of Illinois at Urbana-Champaign, Urbana, Illinois, 61801, USA*

[2]*Nick Holonyak, Jr Micro and Nanotechnology Laboratory, University of Illinois at Urbana-Champaign, Urbana, Illinois, 61801, USA*

This file includes:

- Discussion
- Figure S1
- Figure S2
- Figure S3

[a] Innovative COmpound semiconductoR LABoratory (ICORLAB); Email: cbayram@illinois.edu; Webpage: https://icorlab.ece.illinois.edu; Phone: +1 (217) 300-0978; Fax: +1 (217) 244-6375

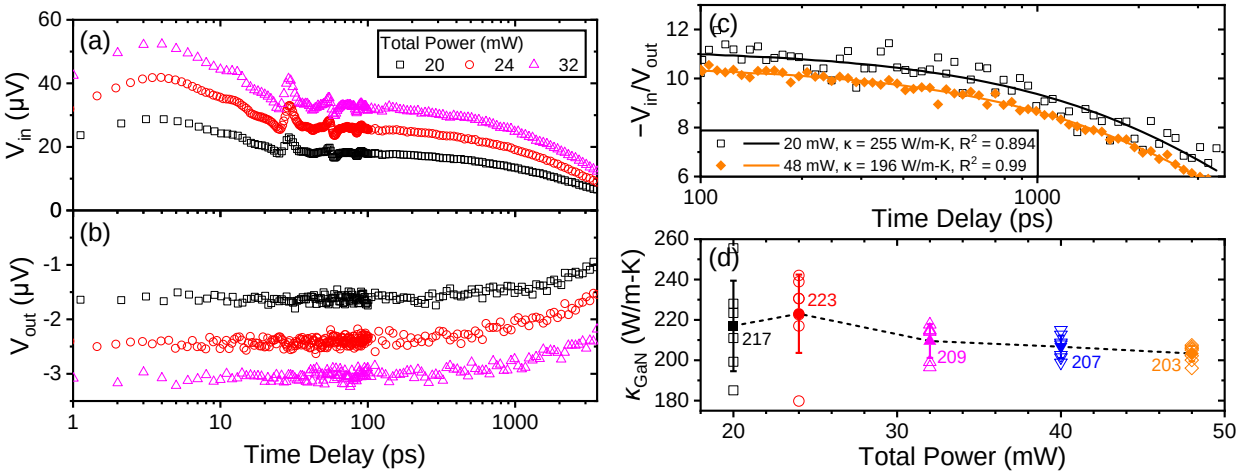

Figure S1. The (a) in-phase signal V_{in}, (b) out-of-phase signal V_{out}, (c) ratio $-V_{in}/V_{out}$ and their fitting results, and (d) thermal conductivity from multiple measurements and their average values with five different laser powers (20, 24, 32, 40, and 48 mW) of TDTR measurement results of HNP GaN are shown. With larger power, noise signals included in the relatively small out-of-phase signal less affects the analysis of the ratio.

Figure S1 shows TDTR measurement data of the HNP GaN sample with different laser powers (black, red, magenta, blue, and orange correspond to total powers of 20, 24, 32, 40, and 48 mW, respectively). Plotted in (a) and (b) are the V_{in} and V_{out} signals, respectively, recorded with a total power of 20, 24, and 32 mW. The pump and probe powers are typically set equal. In short time delays (< 100 ps), the signals are recorded with smaller intervals (0.5 ps) to determine h_{Al} with high accuracy. In an ideal case, the power of the pump and probe beams should not affect the fitting result since the ratio $-V_{in}/V_{out}$ is analyzed. However, due to signal noise (mostly in the V_{out}), increasing the total power up to a level where the ratio is not severely distorted by the noise is practical for reducing the error in thermal conductivity extraction. Figure S1 (c) shows the ratio data (symbols) and model calculation (solid lines) for powers of 20 and 48 mW. The goodness of fitting assessed by the coefficient of determination R^2 is significantly larger for the measurement using 48 mW laser power. More importantly, the extracted thermal conductivity shows a 30% difference between the two measurements. Figure S1 (d) shows the measured thermal conductivity with different laser powers. The average thermal conductivities (filled symbols) for each power and thermal conductivity extracted from each measurement (open symbols) are shown together. Measurements are done on the same spot of the sample while keeping all conditions unchanged except for the laser powers. With increasing power, the standard deviation is reduced. As the total power is increased from 20 to 24 mW, the average thermal conductivity increases due to the improved signal-to-noise ratio, but the standard deviation is still quite large; with power of 24 mW, lowest and highest thermal conductivities measured are 180 and 255 W/m-K, respectively. With powers larger than 30 mW, the standard deviations are small (< 5 %) and the coefficient of determination for each fitting is consistently larger than $R^2 > 0.96$. However, also observed is a slight gradual decrease of thermal conductivity which we attribute to the steady-state heating of the material. Thus, in our measurements, considering the goodness of fitting, standard deviation in measured thermal conductivity, and the steady-state heating, a power of 32 mW is selected.

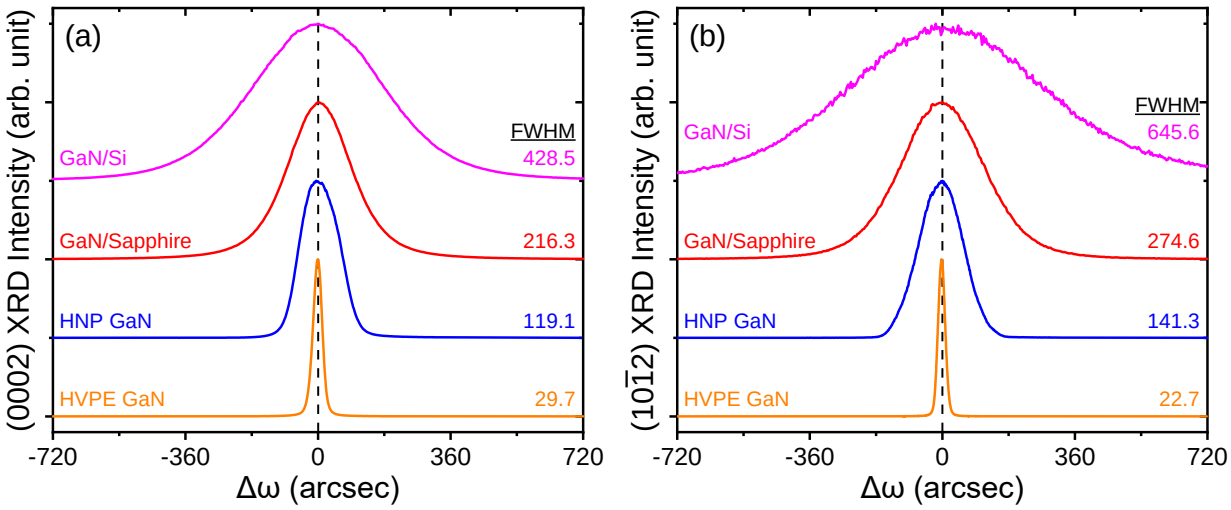

Figure S2. Representative XRD ω scans in the (a) (0002) symmetric and (b) (10$\bar{1}$2) asymmetric planes are performed for the HVPE GaN, HNP GaN, GaN/sapphire, and GaN/Si samples (shown in magenta, red, blue, and orange, respectively). FWHM of the ω scans are extracted and used to estimate the dislocation density of each sample. Multiple scans are performed for each sample to obtain an average value.

Figure S2 shows representative XRD ω scans (rocking curves) in the (a) (0002) symmetric and (b) (10$\bar{1}$2) asymmetric planes of the HVPE GaN, HNP GaN, GaN/sapphire, and GaN/Si samples. Based on the FWHM of the rocking curves, the screw-type dislocation density σ_{screw} and the edge-type dislocation density σ_{edge} are calculated by the relations:[1]

$$\sigma_{screw} = \frac{\beta_{(0002)}^2}{4.35 b_{screw}^2} \quad (1)$$

$$\sigma_{edge} = \frac{\beta_{(10\bar{1}2)}^2 - \beta_{(0002)}^2}{4.35 b_{edge}^2} \quad (2)$$

where $\beta_{(0002)}$ and $\beta_{(10\bar{1}2)}$ are the FWHM (in units of rad) of the (0002) and (10$\bar{1}$2) rocking curves, respectively; b_{screw} = 0.5185 nm and b_{edge} = 0.3189 nm are the Burgers vector length of screw- and edge-type dislocations, respectively. The dislocation densities shown in Table 1 are the summation of the two types of dislocations.

Note that $\beta_{(10\bar{1}2)}$ is larger than $\beta_{(0002)}$ in most cases. For the HVPE GaN, due to the larger $\beta_{(0002)}$ than $\beta_{(10\bar{1}2)}$, Eq. (2) cannot be used. We attribute the failure of using Eqs. (1) and (2) for the HVPE GaN to its low dislocation density.

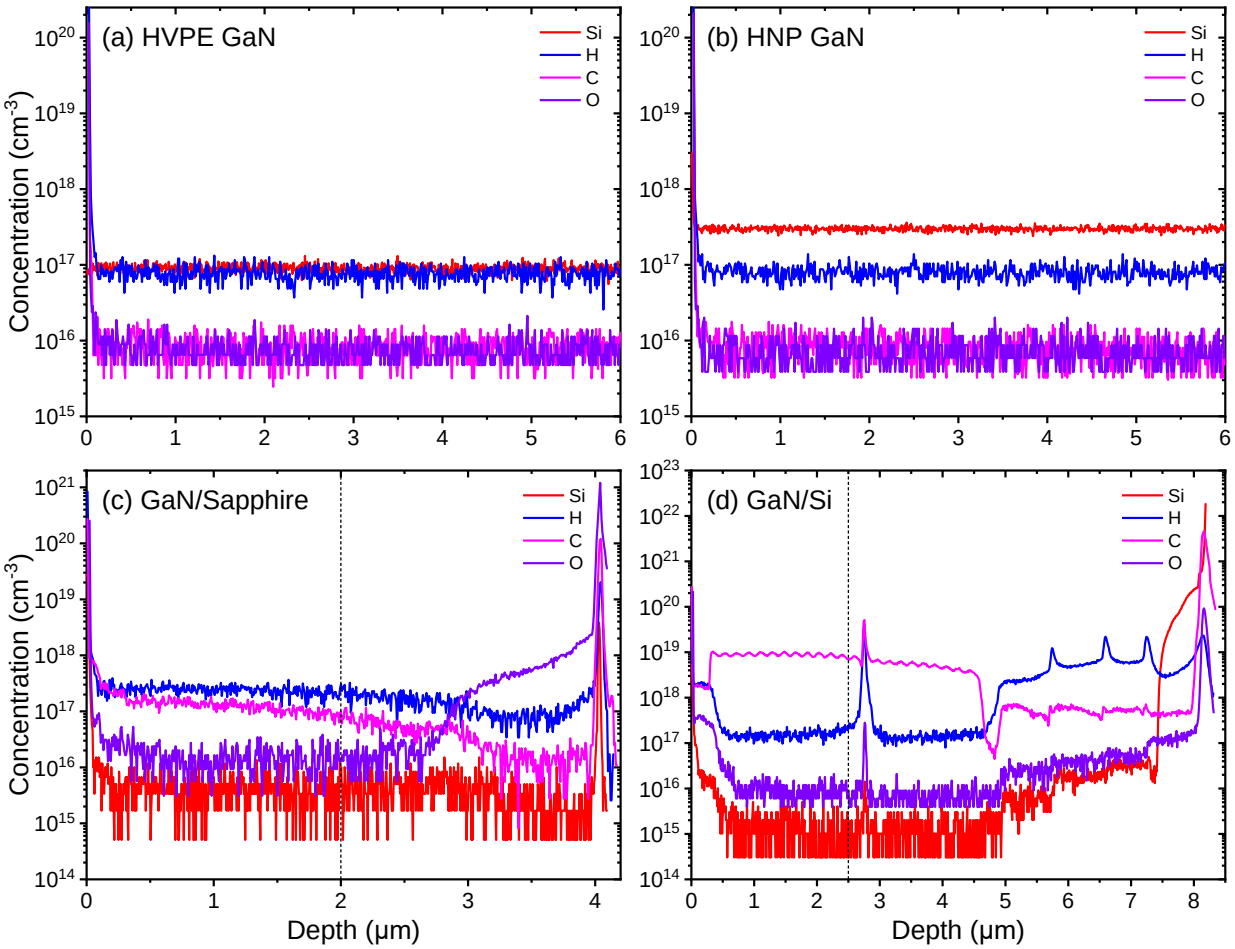

Figure S3. SIMS measurement results of the (a) HVPE GaN, (b) HNP GaN, (c) GaN/sapphire, and (d) GaN/Si samples. Average concentration values of impurities Si, H, C, and O are used in the Klemens' model to calculate the scattering strength Γ between phonons and impurities.

Figure S3 shows the SIMS measurement results of the (a) HVPE GaN, (b) HNP GaN, (c) GaN/sapphire, and (d) GaN/Si samples. Prior to SIMS analysis, a thin layer of Au is used to coat the sample to prevent any sputtering caused surface charging effect. The analysis is performed by a CAMECA secondary ion mass spectrometer. The instrument applies a cesium ion beam with 14.5 keV energy to sputter the sample surface, after which the negative secondary atomic ions such as Si, H, C, and O, are captured by the detector. The detection limits of the Si, H, C, and O ions are 1×10^{15}, 7×10^{16}, 5×10^{15}, and 5×10^{15} cm^{-3}, respectively. Except for Si in the (c) GaN/sapphire and (d) GaN/Si samples, the concentrations of impurities are well above the detection limit.

The impurity concentrations listed in Table 1 are averaged values. The first (top) 0.3 μm of the profile is excluded in taking the average concentration. Also, for the (c) GaN/sapphire and (d) GaN/Si samples, only up to the depth of 2 μm and 2.5 μm, respectively, are considered. With the modulation frequency of 11 MHz used in our TDTR setting, the thermal penetration depth is less than 2 μm assuming the thermal conductivity of GaN is 200 W/m-K and the volumetric heat capacitance of GaN is 2.64 J/cm^3K. Therefore, only impurities within the top 2 μm will influence

the thermal transport. SIMS analysis results on similar GaN samples reported in literature can be found in Refs. 2, 3, 4, 5.

Through Klemens' model, *scattering strength* parameter Γ is calculated by

$$\Gamma = \sum_i f_i \left[1 - \frac{M_i}{\bar{M}}\right]^2, \tag{3}$$

where f_i is the fractional concentration of the i-th impurity atom, M_i is the atomic mass of the i-th impurity atom, and M is the average atomic mass. The atomic masses of H, C, O, Si, Ga, and N used in the calculation are M_H = 1.00794, M_C = 12.0107, M_O = 15.999, M_{Si} = 28.0855, M_{Ga} = 70.9247, M_N = 14.0031 Da, respectively.

The phonon–isotope scattering process is also quantified using a similar approach:[6,7]

$$\Gamma_{\text{isotope}} = 2\left[\left(\frac{M_{\text{Ga}}}{M_{\text{Ga}} + M_{\text{N}}}\right)^2 \Gamma(\text{Ga}) + \left(\frac{M_{\text{Ga}}}{M_{\text{Ga}} + M_{\text{N}}}\right)^2 \Gamma(\text{N})\right], \tag{4}$$

where Γ_{isotope} is the isotope *scattering strength* parameter; M_{Ga} and M_N are the average atomic mass of Ga and N isotopes, respectively; Γ(Ga) and Γ(N) are calculated by Eq. (3) while only considering isotope atoms of Ga and N (and not impurity atoms), respectively. The naturally occurring isotope compositions of the Ga atom are 60.1 % of ^{69}Ga and 39.9% of ^{71}Ga. For the N atom, the compositions are 99.63% of ^{14}N and 0.37% of ^{15}N. The isotope masses are given as $M(^{69}\text{Ga})$ = 68.9256, $M(^{71}\text{Ga})$ = 70.9247, $M(^{14}\text{N})$ = 14.0031, and $M(^{15}\text{N})$ = 15.0001 Da. The GaN samples used in our measurements are not in any way isotopically enriched, hence, we apply a constant Γ_{isotope} of 2.744×10^{-4} for all samples.

[1] R. Liu, C. McCormick, and C. Bayram, AIP Adv. 9, 025306 (2019).
[2] R. Rounds, B. Sarkar, T. Sochacki, M. Bockowski, M. Imanishi, Y. Mori, R. Kirste, R. Collazo, and Z. Sitar, J. Appl. Phys. 124, 105106 (2018).
[3] T. E. Beechem, A. E. McDonald, E. J. Fuller, A. A. Talin, C. M. Rost, J.-P. Maria, J. T. Gaskins, P. E. Hopkins, and A. A. Allerman, J. Appl. Phys. **120**, 095104 (2016).
[4] P. P. Paskov, M. Slomski, J. H. Leach, J. F. Muth, and T. Paskova, AIP Adv. 7, (2017).
[5] G. Parish, S. Keller, S. P. Denbaars, and U. K. Mishra, J. Electron. Mater. 29, 15 (2000).
[6] D. T. Morelli, J. P. Heremans, and G. A. Slack, Phys. Rev. B 66, 1953041 (2002).
[7] P. P. Paskov, M. Slomski, J. H. Leach, J. F. Muth, and T. Paskova, AIP Adv. 7, (2017).